Quantum Mechanics with a Momentum-Space Artificial Magnetic Field

Hannah M. Price, Tomoki Ozawa, and Iacopo Carusotto
INO-CNR BEC Center and Dipartimento di Fisica, Università di Trento, I-38123 Povo, Italy
(Received 4 June 2014; published 6 November 2014)

The Berry curvature is a geometrical property of an energy band which acts as a momentum space magnetic field in the effective Hamiltonian describing single-particle quantum dynamics. We show how this perspective may be exploited to study systems directly relevant to ultracold gases and photonics. Given the exchanged roles of momentum and position, we demonstrate that the global topology of momentum space is crucially important. We propose an experiment to study the Harper-Hofstadter Hamiltonian with a harmonic trap that will illustrate the advantages of this approach and that will also constitute the first realization of magnetism on a torus.

DOI: 10.1103/PhysRevLett.113.190403 PACS numbers: 03.65.Vf, 67.85.-d

The Hamiltonian of a charged particle in an electromagnetic field is a familiar and fundamental result in quantum mechanics [1]. In this Hamiltonian,

$$\mathcal{H} = \frac{[\mathbf{p} - e\mathbf{A}(\mathbf{r})]^2}{2M} + e\Phi(\mathbf{r}), \tag{1}$$

the roles of momentum and position are inherently asymmetric; the magnetic vector potential, $\mathbf{A}(\mathbf{r})$, is a function of position which redefines the relationship between the canonical, $\mathbf{p}$, and physical, $\mathbf{p} - e\mathbf{A}(\mathbf{r})$, momenta. The vector potential $\mathbf{A}(\mathbf{r})$ is also responsible for the geometric Aharanov-Bohm phase, which depends on the real-space trajectory of a particle.

The magnetic Hamiltonian has an important *momentum space* counterpart,

$$\tilde{\mathcal{H}} = E(\mathbf{p}) + W(\mathbf{r} + \boldsymbol{\mathcal{A}}(\mathbf{p})), \tag{2}$$

that underlies many intriguing phenomena in solid state physics such as the anomalous [2–4] and spin Hall effects [5–7] as well as peculiar features of graphene [8,9] and bulk Rashba semiconductors [10]. In this formalism, $E(\mathbf{p})$ is the energy dispersion of the band under consideration, while $\boldsymbol{\mathcal{A}}(\mathbf{p})$ is the geometrical Berry connection of the band (defined below) [2,6,11]. The Berry connection acts as a momentum space vector potential, redefining the relationship between the canonical, $\mathbf{r}$, and physical, $\mathbf{r} + \boldsymbol{\mathcal{A}}(\mathbf{p})$, position operators appearing in the external potential term $W(r + \boldsymbol{\mathcal{A}}(\mathbf{p}))$. This replacement has important physical consequences that have been studied primarily, so far, at the semiclassical level [2,3,5–7,12,13]. As in the Aharanov-Bohm effect, a particle moving in momentum space under the influence of an external force gains a geometrical Berry phase due to the connection $\boldsymbol{\mathcal{A}}(\mathbf{p})$. The curvature, $\Omega(\mathbf{p}) = \nabla_{\mathbf{p}} \times \boldsymbol{\mathcal{A}}(\mathbf{p})$, also naturally defines a momentum space magnetic field [6,11,14,15].

Local geometrical properties of energy bands can be related to global topological invariants. For example, the simplest topological invariant of a 2D crystal, the so-called Chern number $\mathcal{C}$, is the integral of the Berry curvature over the first Brillouin zone (BZ). In the analogy with magnetism, the Chern number is the momentum space counterpart of the number of magnetic monopoles [16] inside a torus. This important invariant underlies the quantization of conductance in the quantum Hall effect [17], while other topological invariants can be defined to classify topological insulators [18,19].

In the last few years, geometrically nontrivial bands have been created in ultracold gases [20–23] and photonic systems [24–27]. Nonzero $\Omega(\mathbf{p})$ can have consequences for the collective modes of an ultracold atomic gas [28,29] and for the semiclassical dynamics of a wave packet [30–35], while the hallmarks of nontrivial topological bands have been observed in topologically protected photonic edge states [24–26].

In this Letter, we discuss how the momentum space magnetic Hamiltonian [Eq. (2)] can be exploited as a fully quantum theory to understand the quantum mechanics of single particles in energy bands with nontrivial geometrical and topological properties, in the presence of additional external potentials. To illustrate this most clearly, we focus on the example of a two-dimensional system where the energy and the Berry curvature of the lowest band are nearly flat over the first BZ. In the presence of an external harmonic potential, the equispaced eigenstates are then the momentum space counterpart of Landau levels in a constant magnetic field. Remarkably, these eigenstates have novel features directly stemming from the global toroidal topology of the BZ. The recent experimental realizations of the Harper-Hofstadter model in ultracold gases [22,23], photonic systems [26], and solid-state superlattices [36] suggest a prompt experimental implementation of our approach. This would open up new avenues to experimentally investigate quantum mechanics and quantum

magnetism on a topologically nontrivial manifold such as a torus [37,38].

The effective quantum Hamiltonian.—We start by presenting a short derivation of the momentum space magnetic Hamiltonian [Eq. (2)] in modern terms for systems of current experimental interest. Our derivation builds on ideas over the last 60 years [2,11,39] and is applicable to the generic single-particle Hamiltonian, $\mathcal{H} = \mathcal{H}_0 + W(\mathbf{r})$, whose first term, $\mathcal{H}_0$, is either translationally invariant or periodic in real space. For example, $\mathcal{H}_0$ could refer to an electron in a crystal, an atom with spin-orbit coupling, an ultracold atomic gas in an optical lattice, or light in either a photonic crystal or a lattice of coupled resonators or waveguides. The second part of the Hamiltonian, $W(\mathbf{r})$, is a weaker additional potential. This could be, for instance, an external static electric field for an electron, a harmonic trap or optical superlattice potential for atoms, or a slow modulation of the background refractive index and/or of the cavity size in optical systems.

The eigenfunctions of $\mathcal{H}_0$ are $|\chi_{n,\mathbf{p}}(\mathbf{r})\rangle = (e^{i\mathbf{p}\cdot\mathbf{r}}/\sqrt{V})|n\mathbf{p}\rangle$, where $|n\mathbf{p}\rangle$ is the energy eigenstate for band index n and momentum $\mathbf{p}$, and V is a normalization factor. If $\mathcal{H}_0$ is periodic, the eigenstate is the periodic Bloch function, $u_{n,\mathbf{p}}(\mathbf{r})$, and the momentum is the crystal momentum defined in the BZ (we take $\hbar = 1$ throughout). The normalization, V, is the number of lattice sites, N. If instead $\mathcal{H}_0$ is translationally invariant, the eigenstate $|n\mathbf{p}\rangle$ is independent of position and V is the volume of the system. For simplicity, we focus on two dimensions, although the extension to 3D is straightforward.

The energy bands have a band structure, $E_n(\mathbf{p})$, and geometrical properties encoded in the Berry connection, $\boldsymbol{\mathcal{A}}_n(\mathbf{p})$, and Berry curvature, $\Omega_n(\mathbf{p})$ [11,40]:

$$\boldsymbol{\mathcal{A}}_n(\mathbf{p}) \equiv i\langle n\mathbf{p}|\frac{\partial}{\partial\mathbf{p}}|n\mathbf{p}\rangle, \qquad \Omega_n(\mathbf{p}) \equiv \nabla_{\mathbf{p}} \times \boldsymbol{\mathcal{A}}_n(\mathbf{p}) \cdot \hat{\mathbf{z}}.$$

The additional potential, $W(\mathbf{r})$, mixes different eigenstates, $|n\mathbf{p}\rangle$. We expand the eigenstates of the full Hamiltonian, $\mathcal{H}$, as $|\Psi\rangle = \sum_n \sum_{\mathbf{p}} \psi_n(\mathbf{p})|\chi_{n,\mathbf{p}}\rangle$, where $\psi_n(\mathbf{p})$ are expansion coefficients. For a periodic $\mathcal{H}_0$, this sum is taken over the first BZ, otherwise, the sum runs over all momenta. We substitute into the Schrödinger equation, $i(\partial/\partial t)|\Psi\rangle = \mathcal{H}|\Psi\rangle$, and apply $\langle\chi_{n',\mathbf{p}'}|$, to obtain:

$$i\frac{\partial}{\partial t}\psi_n(\mathbf{p}) = E_n(\mathbf{p})\psi_n(\mathbf{p}) + \sum_{n,\mathbf{p}}\langle\chi_{n',\mathbf{p}'}|W(\mathbf{r})|\chi_{n,\mathbf{p}}\rangle\psi_n(\mathbf{p}).$$

We expand $W(\mathbf{r})$ as a power series in $\mathbf{r}$, and repeatedly insert the completeness relation: $1 = \sum_n \sum_{\mathbf{p}} |\chi_{n,\mathbf{p}}\rangle\langle\chi_{n,\mathbf{p}}|$ (demonstrated explicitly in the Supplemental Material [41] for a harmonic trap). Then we can use the identity:

$$\langle\chi_{n',\mathbf{p}'}|\mathbf{r}|\chi_{n,\mathbf{p}}\rangle = \delta_{\mathbf{p},\mathbf{p}'}\left(\delta_{n,n'}i\nabla_{\mathbf{p}} + i\langle n'\mathbf{p}'|\frac{\partial}{\partial\mathbf{p}}|n\mathbf{p}\rangle\right),$$

which we have generalized from a previously known result [2,39]. We assume that the additional potential is sufficiently weak that it does not significantly mix energy bands and that the contribution from only one band n is nonnegligible. A quantitative condition for this approximation will be discussed in the following. The effective quantum Hamiltonian in the single-band approximation then has the form [Eq. (2)] with the suitable $E_n(\mathbf{p})$ and $\boldsymbol{\mathcal{A}}_n(\mathbf{p})$. Of course, this Hamiltonian may be generalized to systems with degeneracies such as graphene and topological insulators [18,19]; then, the effective momentum space magnetic field has a non-Abelian gauge structure [6,45].

Connections with magnetism.—The duality between momentum space magnetism and real space magnetism is transparently demonstrated by comparing the effective Hamiltonian [Eq. (2)] to the textbook magnetic Hamiltonian [Eq. (1)]. The energy bandstructure, $E_n(\mathbf{p})$, acts like the external scalar potential $e\Phi(\mathbf{r})$, while the external potential $W[i\nabla_{\mathbf{p}} + \boldsymbol{\mathcal{A}}_n(\mathbf{p})]$ corresponds to the "kinetic energy", $(1/2M)[\mathbf{p} - e\mathbf{A}(\mathbf{r})]^2$ [46]. For a harmonic trapping potential, $W(\mathbf{r}) = \frac{1}{2}\kappa\mathbf{r}^2$, the effective Hamiltonian [Eq. (2)] is:

$$\tilde{\mathcal{H}} = E_n(\mathbf{p}) + \frac{\kappa[i\nabla_{\mathbf{p}} + \boldsymbol{\mathcal{A}}_n(\mathbf{p})]^2}{2}, \tag{3}$$

where the inverse trapping strength, κ^{-1} acts as the particle mass, M. (This is further illustrated in the Supplemental Material [41] for the toy model of a harmonic trap in an optical lattice without a momentum space magnetic field.) We focus hereafter on $W(\mathbf{r}) = \frac{1}{2}\kappa\mathbf{r}^2$, but other forms of the energy-momentum relationship in the real space magnetic Hamiltonian could be obtained by applying different types of external potential, $W(\mathbf{r})$.

The topology of momentum space.—The global properties of the Berry connection and curvature have been deeply investigated as they are related to topological invariants, underlying, for example, the quantum Hall effect [17]. However, much less attention has been devoted to the impact of the global topology of momentum space on the particle wave function which must be single valued [1]. This condition is irrelevant when the momentum $\mathbf{p}$ can take arbitrarily large values, e.g., for particles with 2D Rashba spin-orbit coupling in a Zeeman field [29], but has very interesting consequences in spatially periodic systems where the momentum is defined over the BZ, which has the topology of a torus. As a concrete example of this, we investigate the Harper-Hofstadter Hamiltonian [48] with an external harmonic trap; this is a natural extension of recent experimental advances [22,23,26,36].

The Harper-Hofstadter model.—In the Harper-Hofstadter model, a particle hops on a 2D lattice in a perpendicular (real or artificial) magnetic field, $\boldsymbol{B} = B\hat{\mathbf{z}}$. In the Landau gauge, $\mathbf{A}(\mathbf{r}) = Bx\hat{\mathbf{y}}$, the tight-binding Hamiltonian with a harmonic trap is:

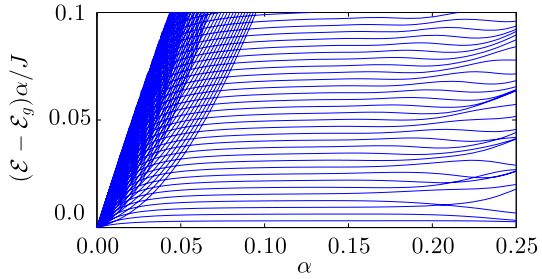

FIG. 1 (color online). The numerical energy spacing relative to the lowest eigenvalue, $\mathcal{E}_g$, for the lowest 100 states, obtained by diagonalizing Eq. (4) for $\kappa a^2/J = 0.02$ and a lattice with $N = 41 \times 41$ sites. The energy spacing is multiplied by α to highlight the spacing of toroidal Landau levels in the lowest band.

$$\mathcal{H} = \mathcal{H}_0 + \frac{1}{2}\kappa a^2 \sum_{m,n} (m^2 + n^2)\hat{a}^\dagger_{m,n}\hat{a}_{m,n},$$
$$\mathcal{H}_0 = -J\sum_{m,n}(\hat{a}^\dagger_{m+1,n}\hat{a}_{m,n} + e^{i\phi}\hat{a}^\dagger_{m,n+1}\hat{a}_{m,n}) + \text{H.c.}, \qquad (4)$$

where $\mathcal{H}_0$ is the Harper-Hofstadter Hamiltonian, J is the hopping amplitude, a is the lattice spacing, and the $\hat{a}^\dagger_{m,n}$ ($\hat{a}_{m,n}$) operators create (annihilate) a particle at lattice site (m, n). The hopping along $\hat{\mathbf{y}}$ is modified by a complex phase $\phi = 2\pi\alpha ma$, where α is the number of magnetic flux quanta per plaquette of the lattice.

Without a harmonic trap, the eigenstates are those of the Harper-Hofstadter Hamiltonian, with behavior governed by the value of α. When $\alpha = p/q$, the tight-binding band splits into q magnetic subbands. The energy spectrum is the well-known Hofstadter butterfly [48]. The magnetic vector potential, $\mathbf{A}(\mathbf{r})$, is not periodic, and the usual translation operators do not commute with $\mathcal{H}_0$ [31]. To apply Bloch's theorem, we define new magnetic translation operators and a larger magnetic unit cell of q plaquettes, that contains an integer number of magnetic flux quanta. The Bloch states are then *magnetic* Bloch states defined within the *magnetic* Brillouin zone (MBZ): $-\pi/a < p_y \leq \pi/a$ and $-\pi/qa < p_x \leq \pi/qa$ (for a magnetic unit cell of q plaquettes along $\hat{\mathbf{x}}$) [31].

Numerical calculations with a harmonic trap.—Adding a harmonic trap splits the Harper-Hofstadter bands into a complicated structure first noted in Ref. [49] and replotted here in Fig. 1 in terms of the energy level spacing relative to the lowest numerical eigenstate. For each value of α, the spectrum was obtained by numerically diagonalizing the full Hamiltonian [Eq. (4)]. The only significant error is from the restriction of Eq. (4) to a finite lattice. To control this, we ensure that all energies are converged to within the accuracy shown. Numerical diagonalization also gives the real space eigenstates of Eq. (4); we relate these to the population in the MBZ via a procedure described in the Supplemental Material [41].

Analytical interpretation.—To understand the complicated spectrum, we build a simple model, focusing on $\alpha = 1/q \ll 1$, where our interpretation is the clearest. In this regime, we can make two simplifications; firstly, with decreasing $\alpha = 1/q$, the bands flatten compared to the hopping energy J. If the bandwidth is much smaller than the harmonic trapping energy, we can assume $E_n(\mathbf{p}) \simeq E_n$, contributing only an overall energy shift. Secondly, when $\alpha = 1/q$ and q is odd, the Chern number of each band, except the middle band, is -1. For $\alpha \ll 1$, the Berry curvature of these bands is increasingly uniform, $\Omega_n(\mathbf{p}) \simeq \Omega_n$ [33,50,51]. The average value, $|\Omega_n| = a^2/(2\pi\alpha)$, is estimated by noting that the Chern number: $\mathcal{C}_n = (1/2\pi)\Omega_n A_{\text{BZ}} = -1$, where $A_{\text{BZ}} = (2\pi)^2/qa^2$ is the area of the MBZ [29]. Therefore for $\alpha = 1/q \ll 1$, the effective Hamiltonian [Eq. (2)] describes a particle in a uniform magnetic field on a torus in momentum space, with an additional overall energy shift.

From the duality between real space and momentum space magnetism, we can translate known analytical results for Eq. (1) to find the eigenspectrum and eigenstates of Eq. (2) [41]. In a real space uniform magnetic field, the eigenstates are Landau levels [1]. Restricting the particle to the surface of a torus, the infinitely degenerate Landau levels are superposed to satisfy the appropriate boundary conditions [37,38].

Including the different Harper-Hofstadter bands, the resulting eigenspectrum of our model can be summarized as a collection of intertwined semi-infinite ladders,

$$\mathcal{E}_{n,\beta} = E_n + \left[\beta + \frac{1}{2}\right]\kappa|\Omega_n|. \qquad (5)$$

Each ladder starts at the energy E_n of the band. Within each ladder, the states are classified by the Landau level quantum number $\beta = 0, 1, 2, \ldots$ and their constant spacing is set by the analog $\kappa|\Omega_n|$ of the cyclotron frequency $\omega_c = e|B|/M$. This is the well-known Landau level spectrum, unaffected by the toroidal topology. However, the topology does reduce the degeneracy of states from an infinite to a finite number, equal to the number of magnetic flux quanta inside the torus [37]. Counting this degeneracy may provide another experimental tool to directly measure the Chern number of nondegenerate bands.

We also translate toroidal Landau levels from real space [38] to the MBZ to find the expected analytical eigenstates (Supplemental Material [41]). The Landau levels are strongly affected by global topology as, for example, their form depends on the Chern number, and the toroidal boundary conditions break translational symmetry in momentum space.

Comparison of numerical and analytical eigenspectra.—Our analytical interpretation is confirmed by numerics, as shown in Fig. 1 over a suitable range of α. Landau levels in the lowest band are spaced by $\kappa|\Omega_0| = \kappa a^2/(2\pi\alpha)$ [Eq. (5)]. Multiplying by α, this energy spacing is a constant (equal to $\simeq 0.003J$ for $\kappa a^2/J = 0.02$). Numerically, this behavior is represented by the almost flat, equispaced states that are visible in Fig. 1 around

$\alpha = 0.1$. The level spacing was noted in Ref. [49] but its origin was not discussed. The eigenstates are nondegenerate as $|C_0| = 1$.

At higher energies in Fig. 1, a second ladder of states cuts across the first. These can be identified as Landau levels in the second lowest Harper-Hofstadter band. (As the spacing is calculated relative to $\mathcal{E}_g$, only states from the lowest Harper-Hofstadter band are horizontal.) The strength of anticrossings between different states is controlled by band mixing from the external harmonic trap. For a sufficiently weak trap and a large band gap, the single-band approximation is valid and levels originating from different bands freely cross without significant coupling. This describes, for example, $\kappa a^2/J = 0.02$ at $\alpha = 1/11$, where the band gap is $(E_1 - E_0)/J \simeq 1$, and the effective Hamiltonian applies to each band separately. The breakdown of this behavior for a stronger trap is discussed in the Supplemental Material [41].

As $\alpha \to 0$, the Harper-Hofstadter bands become too close and band mixing is important. In this limit, the energies are those of a 2D simple harmonic oscillator on a tight-binding lattice [49]. As this is independent of α, the numerical quantity plotted in Fig. 1 vanishes for all states. In the opposite limit, as $\alpha \gtrsim 0.2$, the energy spacing becomes distorted as we can no longer approximate $\Omega_n(\mathbf{p})$ and $E_n(\mathbf{p})$ as uniform: two assumptions which simplified the effective Hamiltonian.

Note that although our analytics are restricted to $\alpha = 1/q$, numerically, the spectrum continuously depends on α. The analytical explanation of this in the general $p > 1$ case requires application of the magnetic model to (almost) degenerate bands with non-Abelian Berry connection, which will be the subject of a future publication.

Comparison of numerical and analytical eigenstates.—Figure 2 shows the 9th and 48th numerical states in real space (a) and (c), and as a population over energy bands in the MBZ (b) and (d). The latter are in excellent agreement with the analytical $\beta = 8$ toroidal Landau level in the $n = 0$, 1 Harper-Hofstadter bands, as demonstrated quantitatively in Fig. 2(e). This agreement supports the single-band approximation, as our analytical wave function is able to capture all numerical features.

The population in the MBZ is mostly determined by the Landau level quantum number β, with a number of nodes that appears to increase with β as expected. The population is also nearly identical in the two bands [see panels (b) and (d)]. Conversely, the real space wave functions, shown in panels (a) and (c), are markedly different, for example, with more nodes as the band index, n, increases. This difference is because the real space states depend on the n via the Bloch wave functions $u_{n,\mathbf{p}}(\mathbf{r})$.

Experimental considerations.—We observe that the form of the Landau levels is remarkably robust to parameter variation, making our proposal well suited to experimental investigation. According to our numerics, the basic features of the lowest energy toroidal Landau levels survive up to

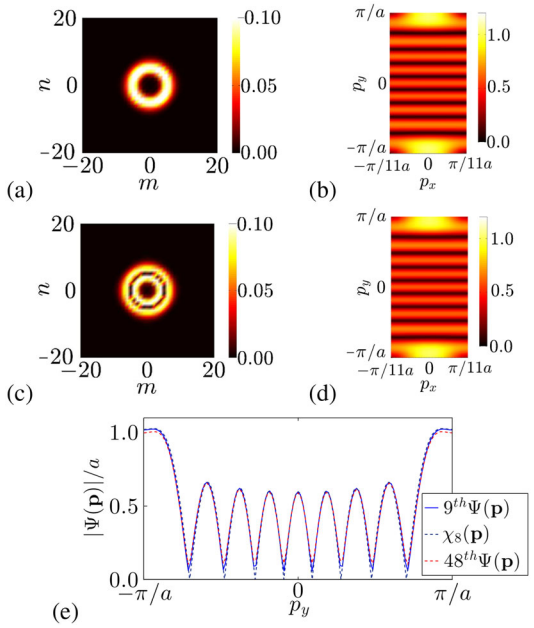

FIG. 2 (color online). The top (middle) row is the 9th (48th) lowest eigenstate of Eq. (4) for $\alpha = 1/11$, $\kappa a^2/J = 0.02$, and a lattice of $N = 133 \times 133$ sites. (a) and (c) The numerical wave function, $|\psi(\mathbf{r})|$, in units of a^{-1}. (b) and (d) The numerical population over bands in the MBZ in units of a. (b) and (d) are qualitatively indistinguishable from the analytical $\beta = 8$ toroidal Landau level, $\chi_8(\mathbf{p})$, in the lowest and second lowest Harper-Hofstadter band, respectively. In both bands, $|\Omega| = a^2/(2\pi\alpha)$ and toroidal Landau levels have the same form (Supplemental Material [41]). (e) Quantitative comparison along $p_x = 0$ taken from (b),(d), and the analytical $\beta = 8$ level.

$\alpha = 1/3$, provided that the harmonic trapping strength is larger than the bandwidth of the lowest band. Importantly, these results are also very insensitive to lattice size, due to strong localisation of the low energy eigenstates in real space (Fig. 2). This is because toroidal Landau levels vary over a large characteristic momentum scale, $l_{\Omega_n} = \sqrt{1/|\Omega_n|}$, which depends only on α and $\mathcal{C}_n$, and which is the analogue of the "magnetic length", $l_B = \sqrt{1/e|B|}$. For relevant parameters here (as well as typical parameters in more general systems), the wave function is delocalized in momentum, and hence, localized in real space (Supplemental Material [41]).

To realize the proposed experiment, a harmonic trap can be straightforwardly added to an ultracold gas using additional laser beams and/or magnetic fields. The momentum space eigenstate structure can be probed directly in time-of-flight measurements of the momentum distribution when both the lattice and artificial magnetic field responsible for the complex hopping terms in [Eq. (4)] are suddenly switched off. While the real space wave function [Figs. 2(a) and 2(c)] is independent of the magnetic gauge choice, the momentum space wave function is not. However, in this experimental procedure, the canonical momentum is measured directly as the physical momentum in the final time-of-flight expansion

stage [22,23,52]. In photonics, similarly, a harmonic potential can be created in the cavity arrays of Refs. [26] and [27] by letting the cavity size vary spatially, while the real (momentum) space wave function can be extracted from the near-field (far-field) emitted light [27,53].

Summary.—We have introduced how future experiments may use external potentials and geometrical energy bands to design novel magnetic Hamiltonians in momentum space. As a first step, we have shown how a particle in a uniform magnetic field confined to a torus may be realized experimentally. The global toroidal topology has important consequences, for example, in the degeneracy of the eigenspectrum, in the spontaneous breaking of translational symmetry in momentum space and in the form of eigenstates.

We are grateful to N. R. Cooper for helpful comments and to P. Ghiggini for mathematical support. This work was partially funded by ERC through the QGBE grant and by the Autonomous Province of Trento, Call "Grandi Progetti 2012," project "On silicon chip quantum optics for quantum computing and secure communications - SiQuro".

[1] L. D. Landau and L. M. Lifshitz, in *Quantum Mechanics*, 3rd ed. (Butterworth-Heinemann, Oxford, 1958), Vol. 3.
[2] E. N. Adams and E. I. Blount, J. Phys. Chem. Solids **10**, 286 (1959).
[3] N. Nagaosa, J. Sinova, S. Onoda, A. H. MacDonald, and N. P. Ong, Rev. Mod. Phys. **82**, 1539 (2010).
[4] F. D. M. Haldane, Phys. Rev. Lett. **93**, 206602 (2004).
[5] S. Murakami, N. Nagaosa, and S.-C. Zhang, Science **301**, 1348 (2003).
[6] K. Y. Bliokh and Y. P. Bliokh, Ann. Phys. (Amsterdam) **319**, 13 (2005).
[7] T. Fujita, M. B. A. Jalil, S. G. Tan, and S. Murakami, J. Appl. Phys. **110**, 121301 (2011).
[8] K. S. Novoselov, A. K. Geim, S. V. Morozov, D. Jiang, M. I. Katsnelson, I. V. Grigorieva, S. V. Dubonos, and A. A. Firsov, Nature (London) **438**, 197 (2005).
[9] Y. B. Zhang, Y. W. Tan, H. L. Stormer, and P. Kim, Nature (London) **438**, 201 (2005).
[10] H. Murakawa, M. S. Bahramy, M. Tokunaga, Y. Kohama, C. Bell, Y. Kaneko, N. Nagaosa, H. Y. Hwang, and Y. Tokura, Science **342**, 1490 (2013).
[11] M. V. Berry, Proc. R. Soc. A **392**, 45 (1984).
[12] K. Y. Bliokh, Europhys. Lett. **72**, 7 (2005).
[13] P. Gosselin, F. Ménas, A. Bérard, and H. Mohrbach, Europhys. Lett. **76**, 651 (2006).
[14] T. T. Wu and C. N. Yang, Phys. Rev. D **12**, 3845 (1975).
[15] N. R. Cooper and R. Moessner, Phys. Rev. Lett. **109**, 215302 (2012).
[16] Z. Fang *et al.*, Science **302**, 92 (2003).
[17] D. J. Thouless, M. Kohmoto, M. P. Nightingale, and M. den Nijs, Phys. Rev. Lett. **49**, 405 (1982).
[18] M. Z. Hasan and C. L. Kane, Rev. Mod. Phys. **82**, 3045 (2010).
[19] X.-L. Qi and S.-C. Zhang, Rev. Mod. Phys. **83**, 1057 (2011).
[20] L. Tarruell, D. Greif, T. Uehlinger, G. Jotzu, and T. Esslinger, Nature (London) **483**, 302 (2012).
[21] J. Struck *et al.*, Nat. Phys. **9**, 738 (2013).
[22] M. Aidelsburger, M. Atala, M. Lohse, J. T. Barreiro, B. Paredes, and I. Bloch, Phys. Rev. Lett. **111**, 185301 (2013).
[23] H. Miyake, G. A. Siviloglou, C. J. Kennedy, W. C. Burton, and W. Ketterle, Phys. Rev. Lett. **111**, 185302 (2013).
[24] Z. Wang, Y. Chong, J. D. Joannopoulos, and M. Soljačić, Nature (London) **461**, 772 (2009).
[25] M. C. Rechtsman, J. M. Zeuner, Y. Plotnik, Y. Lumer, D. Podolsky, F. Dreisow, S. Nolte, M. Segev, and A. Szameit, Nature (London) **496**, 196 (2013).
[26] M. Hafezi, S. Mittal, J. Fan, A. Migdall, and J. M. Taylor, Nat. Photonics **7**, 1001 (2013).
[27] T. Jacqmin, I. Carusotto, I. Sagnes, M. Abbarchi, D. D. Solnyshkov, G. Malpuech, E. Galopin, A. Lemaître, J. Bloch, and A. Amo, Phys. Rev. Lett. **112**, 116402 (2014).
[28] E. van der Bijl and R. A. Duine, Phys. Rev. Lett. **107**, 195302 (2011).
[29] H. M. Price and N. R. Cooper, Phys. Rev. Lett. **111**, 220407 (2013).
[30] A. M. Dudarev, R. B. Diener, I. Carusotto, and Q. Niu, Phys. Rev. Lett. **92**, 153005 (2004).
[31] M.-C. Chang and Q. Niu, Phys. Rev. Lett. **75**, 1348 (1995).
[32] H. M. Price and N. R. Cooper, Phys. Rev. A **85**, 033620 (2012).
[33] M. Cominotti and I. Carusotto, Europhys. Lett. **103**, 10001 (2013).
[34] A. Dauphin and N. Goldman, Phys. Rev. Lett. **111**, 135302 (2013).
[35] T. Ozawa and I. Carusotto, Phys. Rev. Lett. **112**, 133902 (2014).
[36] C. R. Dean *et al.*, Nature (London) **497**, 598 (2013).
[37] J. K. Jain, *Composite Fermions* (Cambridge University Press, Cambridge, 2007).
[38] M. H. Al-Hashimi and U.-J. Wiese, Ann. Phys. (Amsterdam) **324**, 343 (2009).
[39] R. Karplus and J. M. Luttinger, Phys. Rev. **95**, 1154 (1954).
[40] D. Xiao, M.-C. Chang, and Q. Niu, Rev. Mod. Phys. **82**, 1959 (2010).
[41] See Supplemental Material http://link.aps.org/supplemental/10.1103/PhysRevLett.113.190403, which includes Refs. [42–44].
[42] M. Krämer, L. Pitaevskii, and S. Stringari, Phys. Rev. Lett. **88**, 180404 (2002).
[43] M. Kohmoto, Ann. Phys. (N.Y.) **160**, 343 (1985).
[44] B. Bernevig and T. Hughes, *Topological Insulators and Topological Superconductors* (Princeton University Press, Princeton, 2013).
[45] F. Wilczek and A. Zee, Phys. Rev. Lett. **52**, 2111 (1984).
[46] Previously discussed specifically for a particle with 2D Rashba spin-orbit coupling in a harmonic trap in Ref. [47].
[47] C. Wu, I. Mondragon-Shem, and X.-F. Zhou, Chin. Phys. Lett. **28**, 097102 (2011).
[48] D. R. Hofstadter, Phys. Rev. B **14**, 2239 (1976).
[49] A. R. Kolovsky, F. Grusdt, and M. Fleischhauer, Phys. Rev. A **89**, 033607 (2014).
[50] J. Zak, Phys. Rev. Lett. **62**, 2747 (1989).
[51] F. Harper, S. H. Simon, and R. Roy, Phys. Rev. B **90**, 075104 (2014).
[52] Y.-J. Lin, R. L. Compton, K. Jiménez-García, W. D. Phillips, J. V. Porto, and I. B. Spielman, Nat. Phys. **7**, 531 (2011).
[53] I. Carusotto and C. Ciuti, Rev. Mod. Phys. **85**, 299 (2013).